

Nonlinear Particle Acceleration in Relativistic Shocks

Donald C. Ellison¹ and Glen P. Double¹

ABSTRACT

Monte Carlo techniques are used to model nonlinear particle acceleration in parallel collisionless shocks of various speed, including mildly relativistic ones. When the acceleration is efficient, the backreaction of accelerated particles modifies the shock structure and causes the compression ratio, r , to change from test-particle values. Modified shocks with Lorentz factors, $\gamma_0 \lesssim 3$, can have compression ratios greater than 4 and the momentum distribution of energetic particles no longer follows a power law relation. For faster shocks, r depends on γ_0 but can drop below 3, giving self-consistent spectra considerably steeper than the so-called ‘universal’ test-particle result of $N(E) \propto E^{-2.3}$. In the ultrarelativistic limit ($\gamma_0 \gtrsim 50$), shocks undergoing efficient particle acceleration may adjust enough to conserve energy and momentum without lowering r and the compression ratio may again approach the test-particle value of 3.

Subject headings: Cosmic rays — acceleration of particles — relativistic shock waves — gamma-ray bursts; PACS: 52.60, 96.40

1. Introduction

Most collisionless shocks in astrophysics are nonrelativistic, i.e., the flow speed of the unshocked plasma in the reference frame at rest with the shock, u_0 , is much less than the speed of light, c . Particle acceleration in such shocks has been studied extensively in both the linear and nonlinear regimes, and we refer the reader to reviews which describe the basic features of the shocks, the energetic particles they produce, and the many applications (e.g., Drury 1983; Blandford & Eichler 1987; Jones & Ellison 1991). Relativistic shocks, where the flow speed Lorentz factor $\gamma_0 = [1 - (u_0/c)^2]^{-1/2}$ is greater than a few, are likely to be much less common than nonrelativistic ones, but may occur in extreme objects such as pulsar winds, hot spots in radio galaxies, and gamma ray bursts (GRBs). Largely motivated by the application to GRBs, relativistic shocks have recently received considerable attention by a number of researchers (e.g., Bednarz & Ostrowski 1996; Kirk et al. 2000; Achterberg et al. 2001). However, except for some preliminary work done over a

¹Department of Physics, North Carolina State University, Box 8202, Raleigh NC 27695, U.S.A.; E-mail: don_ellison@ncsu.edu; gpdouble@unity.ncsu.edu; 919-515-7227

decade ago (Schneider & Kirk 1987; Ellison 1991a,b), current descriptions of relativistic shocks undergoing first-order Fermi acceleration are test particle approximations that do not include the backreaction of the accelerated particles on the shock structure. This may be a serious limitation of relativistic shock theory in applications, such as GRBs, where high particle acceleration efficiencies are often assumed. Here, we present results for nonlinear acceleration where the backreaction of the accelerated population on the relativistic shock structure is included self-consistently.

In collisionless shocks, charged particles gain energy by scattering back and forth between the converging upstream and downstream plasmas. This basic physical process, called diffusive or first-order Fermi shock acceleration, is the same in relativistic and nonrelativistic shocks, but differences in the mathematical description and outcome of the process occur because energetic particle distributions are nearly isotropic in the shock reference frame in nonrelativistic shocks (where $v \gg u_0$; v is the individual particle speed), but are highly anisotropic in relativistic shocks (since $v \sim u_0 \sim c$) (e.g., Peacock 1981). The description of particle diffusion and energy gain is far more difficult when $\gamma_0 \gg 1$ because the diffusion approximation, which requires nearly isotropic distribution functions, cannot be made. Because of this, Monte Carlo simulations, where particle scattering and transport are treated explicitly, and which, in effect, solve the Boltzmann equation with collective scattering (e.g., Ellison & Eichler 1984; Kirk & Schneider 1987b; Ellison, Jones, & Reynolds 1990; Ellison & Reynolds 1991; Ostrowski 1991; Bednarz & Ostrowski 1996), offer advantages over analytic methods. This is true in the test-particle approximation, where analytic results exist, but is even more important for nonlinear relativistic shocks.

In nonrelativistic shocks, for $v \gg u_0$, a diffusion-convection equation can be solved directly (e.g., Axford, Leer, & Skadron 1977; Blandford & Ostriker 1978), yielding the well-known result

$$f(p) d^3p \propto p^{-\sigma} d^3p \quad \text{with} \quad \sigma = 3r/(r-1), \quad (1)$$

where r is the shock compression ratio, p is the momentum, and $f(p) d^3p$ is the number density of particles in d^3p . Equation (1) is a steady-state, test-particle result with an undetermined normalization, but the spectral index, σ , in this limit is independent of the shock speed, u_0 , or any details of the scattering process as long as there is enough scattering to maintain isotropy in the local frame. To obtain an absolute injection efficiency, or to self-consistently describe the nonlinear backreaction of accelerated particles on the shock structure (at least when the seed particles for acceleration are not fully relativistic to begin with), techniques which do not require $v \gg u_0$ must be used. Furthermore, for particles that do not obey $v \gg u_0$ additional assumptions must be made for how these particles interact with the background magnetic waves and/or turbulence, i.e., the so-called “injection problem” must be considered (see, for example, Jones & Ellison 1991; Malkov 1998). The Monte Carlo techniques we describe here make the simple assumption that all particles, regardless of energy, interact in the same way, i.e., all particles scatter elastically and isotropically in the local plasma frame with a mean free path proportional to their gyroradius. These techniques and assumptions have been used to calculate nonlinear effects in nonrelativistic collisionless shocks for a number of years with good success comparing model results to spacecraft observations (e.g., Ellison & Eichler 1984; Ellison, Möbius, & Paschmann 1990; Ellison, Jones, & Baring 1999).

Early work on relativistic shocks was mostly analytical in the test particle approximation (e.g., Blandford & McKee 1976; Peacock 1981; Kirk & Schneider 1987a; Heavens & Drury 1985), although the analytical work of Schneider & Kirk (1987) explored modified shocks. Test-particle Monte Carlo techniques for relativistic shocks were developed by Kirk & Schneider (1987b) and Ellison, Jones, & Reynolds (1990) for parallel, steady-state shocks, i.e., those where the shock normal is parallel to the upstream magnetic field, and extended to include oblique magnetic fields by Ostrowski (1991). Some preliminary work on modified relativistic shocks using Monte Carlo techniques was done by Ellison (1991b,a).

The most important results from the theory of test-particle acceleration in ultrarelativistic shocks are: (i) regardless of the state of the unshocked plasma, particles can pick up large amounts of energy ($E_f/E_i \sim \gamma_0^2$) in their first shock crossing cycle (Vietri 1995), but receive much smaller energy boosts ($< E_f/E_i > \sim 2$) for subsequent crossing cycles (e.g., Gallant & Achterberg 1999; Achterberg et al. 2001)²; (ii) the shock compression ratio, defined as $r \equiv u_0/u_2$, tends to 3 as $u_0 \rightarrow c$ (e.g., Peacock 1981; Kirk 1988), where u_2 is the flow speed of the shocked plasma measured in the shock frame;³ and (iii) a so-called ‘universal’ spectral index, $\sigma \sim 4.2\text{--}4.3$ (in equation 1) exists in the limits of $\gamma_0 \gg 1$ and $\delta\theta \ll 1$, where $\delta\theta$ is the change in direction a particle’s momentum vector makes at each pitch angle scattering (e.g., Bednarz & Ostrowski 1998; Achterberg et al. 2001).

We find that these results are modified in mildly relativistic shocks, even in the test-particle approximation, and in fully relativistic shocks (at least for $\gamma_0 \lesssim 50$) when the backreaction of the accelerated particles is treated self-consistently, which causes the shock to smooth and the compression ratio to change from test-particle values. In mildly relativistic shocks, $f(p)$ remains a power law in the test-particle approximation but both r and σ depend on the shock Lorentz factor, γ_0 . When efficient particle acceleration occurs in mildly relativistic shocks ($\gamma_0 \lesssim 3$), large increases in r can result and a power law is no longer a good approximation to the spectral shape. In these cases, we determine the compression ratio by balancing the momentum and energy fluxes across the shock with the Monte Carlo simulation. For $\gamma_0 \gtrsim 3$, accelerated particles smooth the shock structure just as they do in slower shocks, but r can *decrease* below the test-particle value of 3. Except for shocks having a small range of mildly relativistic Lorentz factors near $\gamma_0 \sim 2.3$, where the transition between $r > 3$ and $r < 3$ occurs, and ultrarelativistic shocks (i.e., $\gamma_0 \gtrsim 50$), efficient particle acceleration can produce spectra very different from the ‘universal’ power law found in the test-particle approximation.

² E_i (E_f) is the particle energy at the start (end) of an upstream to downstream to upstream (or a downstream to upstream to downstream) shock crossing cycle.

³Note that the density ratio across the shock, $\rho_2/\rho_0 \neq u_0/u_2$ as is the case in nonrelativistic shocks, because the Lorentz factors associated with the relativistic flows modify the particle flux jump condition. Here and elsewhere we use the subscript 0 (2) to indicate far upstream (downstream) values.

2. Monte Carlo Model

The techniques we use are essentially identical to those described in Ellison, Baring, & Jones (1996) and Ellison, Jones, & Baring (1999). The differences are that the code has been made fully relativistic and only results for parallel shocks with pitch-angle diffusion are presented here. The code is steady-state, implicitly includes a uniform magnetic field, and moves particles in helical orbits. We assume the Alfvén Mach number is large, i.e., we neglect any effects from Alfvén wave heating in the upstream precursor. This also means we neglect the second-order acceleration of particles scattering between oppositely propagating Alfvén waves. Such an effect in relativistic plasmas with strong magnetic fields is proposed for nonlinear particle acceleration in GRBs by Pelletier (1999) (see also Pelletier & Marcowith 1998).

The pitch angle diffusion is performed as described in (Ellison, Jones, & Reynolds 1990). That is, after a small increment of time, δt , a particles’ momentum vector, \mathbf{p} , undergoes a small change in direction, $\delta\theta$. If the particle originally had a pitch angle, θ (measured relative to the shock normal direction), it will have a new pitch angle θ' such that

$$\cos \theta' = \cos \theta \cos \delta\theta + \sqrt{1 - \cos^2 \theta} \sin \delta\theta \cos \phi , \quad (2)$$

where ϕ is the azimuth angle measured with respect to the original momentum direction. All angles are measured in the local plasma frame. If $\delta\theta$ is chosen randomly from a uniform distribution between 0 and $\delta\theta_{\max}$ and ϕ is chosen from a uniform distribution between 0 and 2π , the tip of the momentum vector will perform a random walk on a sphere of radius p . As shown by Ellison, Jones, & Reynolds (1990), the angle $\delta\theta_{\max}$ is determined by

$$\delta\theta_{\max} = (6 \delta t / t_c)^{1/2} = (12\pi / N)^{1/2} , \quad (3)$$

where $N = \tau_g / \delta t \gg 1$ is the number of gyro-segments, δt , dividing a gyro-period $\tau_g = 2\pi r_g / v$. The time t_c is a “turn around” time defined as $t_c = \lambda / v$, where λ is the particle mean free path. The mean free path is taken to be proportional to the gyroradius $r_g = pc / (QeB)$ (e is the electronic charge, Q is the ionic charge number, and B is the local uniform magnetic field), i.e., $\lambda = \eta r_g$, where η determines the strength of scattering. In all of the examples given here we set $\eta = 1$, or, in other words, the strong scattering Bohm limit is assumed.

For a downstream particle to return upstream, it’s velocity vector must be directed within a cone with opening angle θ_2 such that $|v_2 \cos \theta_2| > u_2$, where v_2 and θ_2 are measured in the downstream frame and $\theta_2 = 0^\circ$ is in the $-x$ -direction, i.e., along the shock normal direction. For ultrarelativistic shocks with $v_2 \simeq c$ and $u_2 \simeq c/3$, $\cos \theta_2 \gtrsim 1/3$ for a downstream particle to cross the shock into the upstream region. When the particle enters the upstream region it will have a high probability of being immediately swept back toward the shock unless it satisfies the more restrictive condition $|v_0 \cos \theta_0| > u_0$, where now v_0 and θ_0 are measured in the upstream frame.⁴

⁴In the test-particle approximation, u_0 is just the shock speed. In nonlinear shocks, the flow speed just upstream

Since both the particle and shock have high Lorentz factors, we can write

$$\cos \theta_0 = u_0/v_0 = \frac{(1 - 1/\gamma_0^2)^{1/2}}{(1 - 1/\gamma_v^2)^{1/2}} \simeq \frac{1 - 1/(2\gamma_0^2)}{1 - 1/(2\gamma_v^2)} , \quad (4)$$

where $\gamma_v \equiv [1 - (v_0/c)^2]^{-1/2}$ is the particle Lorentz factor. Since $\cos \theta_0 \simeq 1 - \theta_0^2/2$ for small θ_0 , we have

$$\theta_0^2 \simeq \frac{1}{\gamma_0^2} - \frac{1}{\gamma_v^2} . \quad (5)$$

For ultrarelativistic particles with $\gamma_v \gg \gamma_0$, $\theta_0 \simeq 1/\gamma_0$ (e.g., Gallant & Achterberg 1999), but θ_0 can be much smaller for mildly relativistic particles.

In order to re-cross into the downstream region, particles must scatter out of the upstream cone defined by θ_0 and Achterberg et al. (2001) show that most particles are only able to change the angle they make with the upstream directed shock normal by $|\delta\theta| \sim \theta_0$ before being sweep back downstream, making the distribution of shock crossing particles highly anisotropic. Therefore, if the shock Lorentz factor $\gamma_0 \gg 1$, a larger fraction of particles re-cross the shock into the downstream region with highly oblique angles (as measured in the shock frame) compared to lower speed shocks (see Figure 2 discussed below). Particles crossing at such oblique angles receive smaller energy gains than would be the case for an isotropic pitch angle distribution and Achterberg et al. (2001) go on to show that $\langle E_f/E_i \rangle \sim 2$ for a shock crossing cycle (after the first one).

Considering these constraints, we require $\delta\theta_{\max} < \theta_0$, or

$$N > N_{\min} = 12\pi\gamma_0^2 , \quad (6)$$

and find (as shown in Figure 1) that the power law spectral index, σ , asymptotically approaches a maximum value as N is increased. If N is less than the value required for convergence (and the gyro-segments are too large), the distribution will be flatter than produced with the convergent value of N because more particles are able to cross from upstream to downstream with $\theta_{\text{sk}} \ll 90^\circ$ and receive unrealistically large energy boosts. This effect has long been known from the comparison of pitch-angle diffusion to large-angle scattering in relativistic shocks (e.g., Kirk & Schneider 1987b; Ellison, Jones, & Reynolds 1990). For all of the examples reported on here, N is chosen large enough so it makes no difference if $\delta\theta$ is chosen uniformly between 0° and $\delta\theta_{\max}$ or if $\cos \delta\theta$ is chosen uniformly between $\cos \delta\theta_{\max}$ and 1. Figure 1 shows how our results depend on N for shock speeds ranging from fully nonrelativistic to fully relativistic. In all cases, as N is increased the spectral index approaches a maximum and for $\gamma_0 \gtrsim 7$ we obtain the well known result $\sigma = 4.2\text{--}4.3$. The fact that the computation time for the Monte Carlo simulation scales as N and $N \propto \gamma_0^2$ places limits on modeling ultrarelativistic shocks with this technique.

from the subshock at $x = 0$ will be less than the far upstream shock speed, u_0 , as measured in the shock reference frame.

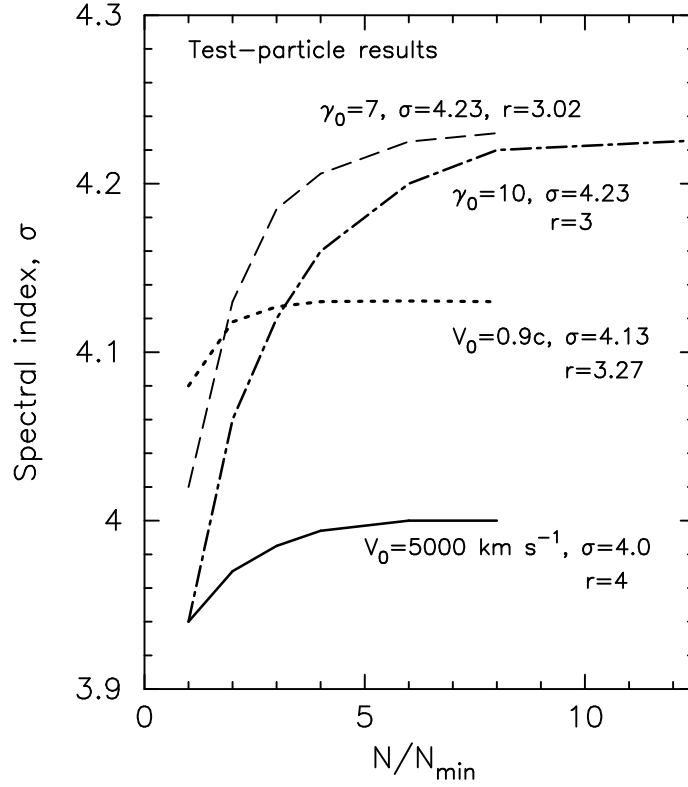


Fig. 1.— Power law spectral index versus number of gyro-segments, N , for various test-particle shocks as labeled. In all cases, as N is increased the spectral index converges and we obtain the two known results of $\sigma \simeq 4$ for nonrelativistic shocks with $r = 4$, and $\sigma \simeq 4.23$ for fully relativistic shocks with $r = 3$. The parameter N_{\min} is defined in equation (6).

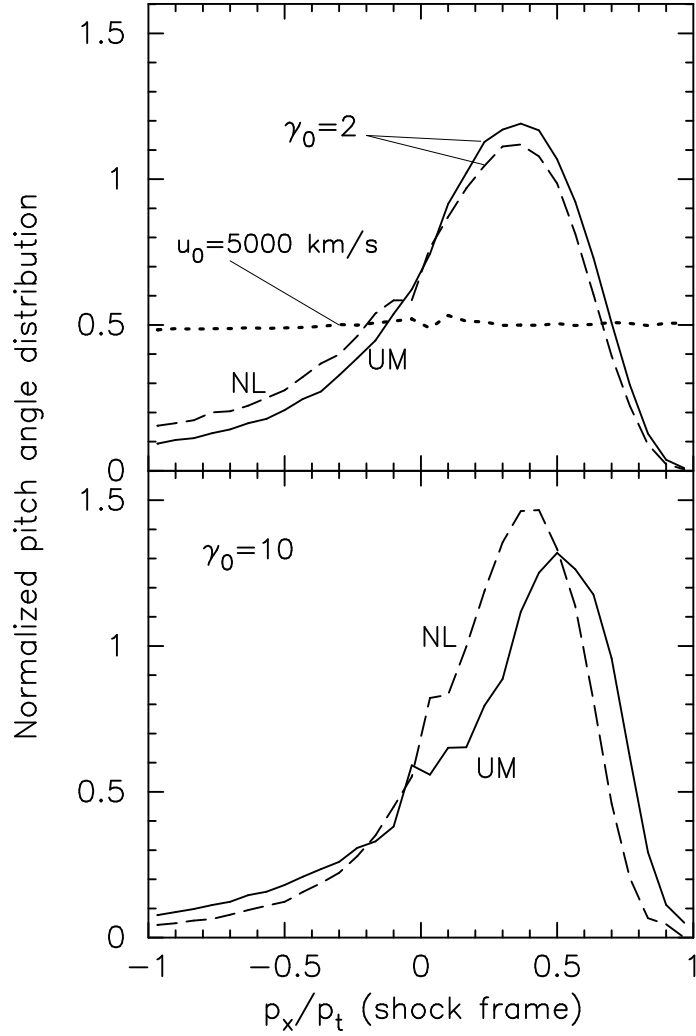


Fig. 2.— Cosine of the pitch angle, i.e., p_x/p_t , for particles crossing $x = 0$. The solid and dashed curves in the top panel are for a shock with Lorentz factor $\gamma_0 = 2$. The dotted curve in the top panel is for a nonrelativistic shock with speed $u_0 = 5000 \text{ km s}^{-1}$. The bottom panel shows curves for a fully relativistic shock with $\gamma_0 = 10$. In all cases, the curves are normalized so that the areas under them is 1 and the x -component of momentum, p_x , is positive when directed downstream. The nonlinear (NL) and unmodified (UM) shock results are labeled.

In Figure 2 we compare pitch-angle distributions (measured in the shock reference frame) of particles crossing the shock. The curves are normalized such that the area under each curve equals one and the x -component of particle momentum in the shock frame, p_x , is positive when directed downstream to the right (see Figure 8 for the shock geometry). Here, p_t is the magnitude of the total particle momentum also measured in the shock frame. In the top panel, we compare an unmodified (UM) and nonlinear (NL) mildly relativistic shock ($\gamma_0 = 2$) with a nonrelativistic one ($u_0 = 5000 \text{ km s}^{-1}$). Particles crossing the $\gamma_0 = 2$ shock are highly anisotropic with p_x/p_t strongly peaked near ~ 0.35 . In the nonrelativistic shock, the particles are nearly isotropic except for a slight flux-weighting effect. There is little difference in the distributions between the UM and NL shocks. In the bottom panel, we show the pitch-angle distributions for UM and NL shocks with $\gamma_0 = 10$. While the distributions are somewhat more sharply peaked, they are quite similar to those for $\gamma_0 = 2$ and show relatively small variations between the UM and NL shocks.

The main difference between our present code and an earlier code used by Ellison, Jones, & Reynolds (1990) to model test-particle relativistic shocks is that the previous code used a guiding center approximation with an emphasis on large-angle scattering rather than the more explicit orbit calculation of pitch-angle diffusion used here. Other than the far greater range in γ_0 and the nonlinear results we now present, the work of Ellison, Jones, & Reynolds (1990) is consistent with the work presented here.

The particle transport is performed as follows. Particles of some momentum, p_{pf} , (measured in the local plasma frame) are injected far upstream from the shock and pitch-angle diffuse and convect until they cross a grid zone boundary, i.e., a dividing plane in the simulation between regions with different bulk flow speeds (see Ellison, Baring, & Jones 1996, for a full discussion). For unmodified shocks there is only one grid zone boundary which divides the upstream and downstream regions, but for nonlinear shocks the bulk flow speed changes in small steps, each separated by a boundary, from u_0 far upstream to u_2 downstream. In the unmodified case, the shock thickness is essentially zero (i.e., shorter than the distance a particle diffuses in δt) but in the nonlinear, modified case, the shock precursor extends over the entire region of varying bulk flow speeds and a small scale “subshock” (at position $x = 0$ in our simulation) exists where most of the entropy production occurs. When a particle crosses a grid zone boundary, p_{pf} is transformed to the new local frame moving with a new speed relative to the subshock and the particle continues to scatter and convect. Each particle is followed until it leaves the system in one of three ways. It can convect far downstream and not return to the subshock, it can obtain a momentum greater than some p_{max} and be removed, or it can diffuse far enough upstream to cross an upstream free escape boundary (FEB) and be removed. Both p_{max} and the position of the FEB are free parameters in our model (see Berezhko & Völk 1997, for a discussion of the self-consistent determination of the maximum particle energy in nonrelativistic supernova remnant shocks). For our nonlinear calculations, we iterate the shock structure and compression ratio until the number, momentum, and energy fluxes are conserved across the shock. This procedure has been detailed many times for nonrelativistic shocks (see Ellison, Baring, & Jones 1996, and references therein) and the modifications required

for relativistic shocks were given in Ellison & Reynolds (1991).

To avoid excessive computation, we use a probability of return calculation as described in detail in Ellison, Jones, & Reynolds (1990). That is, we use the standard expression obtained by Peacock (1981),

$$P_R = \left(\frac{v - u_2}{v + u_2} \right)^2, \quad (7)$$

to determine the probability, P_R , that a particle, having crossed a particular point in the uniform downstream flow, will return back across that point. Equation (7) is fully relativistic and independent of the diffusive properties of the particles as long as they are isotropic in the u_2 frame. We ensure this isotropy by only applying equation (7) once a particle has diffused several mean free paths downstream from the shock. For ultrarelativistic shocks with $v \simeq u_0 \simeq c$ and $r \simeq 3$, equation (7) gives $P_R \simeq 0.25$.

For clarity, we note that this is not the same probability, \mathcal{P}_{ret} , that is used by Achterberg et al. (2001) to determine the test-particle power law index, i.e.,

$$s = 1 + \frac{\ln(1/\mathcal{P}_{\text{ret}})}{\ln \langle E_f/E_i \rangle}, \quad (8)$$

where $N(E) \propto E^{-s}$ and, for fully relativistic particles, $s = \sigma - 2$. The quantity $\langle E_f/E_i \rangle$ is the average energy ratio for a particle undergoing a shock crossing cycle. Although not explicitly stated in Achterberg et al. (2001), it is clear from the context that \mathcal{P}_{ret} is calculated just behind the shock where the particle distribution is highly anisotropic. In this case, particles that have just crossed from upstream to downstream will be more likely to recross back into the upstream region than indicated by equation (7) because their pitch angles are more likely to be highly oblique relative to the shock normal than in the isotropic distributions further downstream (compare the solid or dashed curves to the dotted curve in the top panel of Figure 2 discussed below). For $\gamma_0 = 10$, Achterberg et al. (2001) find $\mathcal{P}_{\text{ret}} = 0.435 \pm 0.005$ and $\langle E_f/E_i \rangle = 1.97 \pm 0.01$ giving the standard result $s = 2.230 \pm 0.012$. As shown in Figure 1, our unmodified results are consistent with this spectral index for $\gamma_0 \gtrsim 7$.

3. Test-Particle Results

In Figure 3 we show particle distributions for unmodified shocks with speeds ranging from fully nonrelativistic ($u_0 = 5000 \text{ km s}^{-1}$) to mildly relativistic ($\beta_0 = u_0/c = 0.5$) to fully relativistic ($\gamma_0 = 10$). The nonrelativistic distribution matches the standard test-particle Fermi result of $\sigma = 4$ for $r = 4$ and the fully relativistic result is consistent with the well-known limit of $\sigma \rightarrow 4.2 - 4.3$ as $\gamma_0 \rightarrow \infty$ for $r = 3$. In the trans-relativistic regime, both the compression ratio and the spectral index vary with u_0 and no known analytic result exists relating them. For the $u_0 = 0.5c$ distribution shown in Figure 3, we have determined the compression ratio by balancing the mass, momentum, and energy fluxes across the shock in the test-particle limit, i.e., by ignoring any effects from the

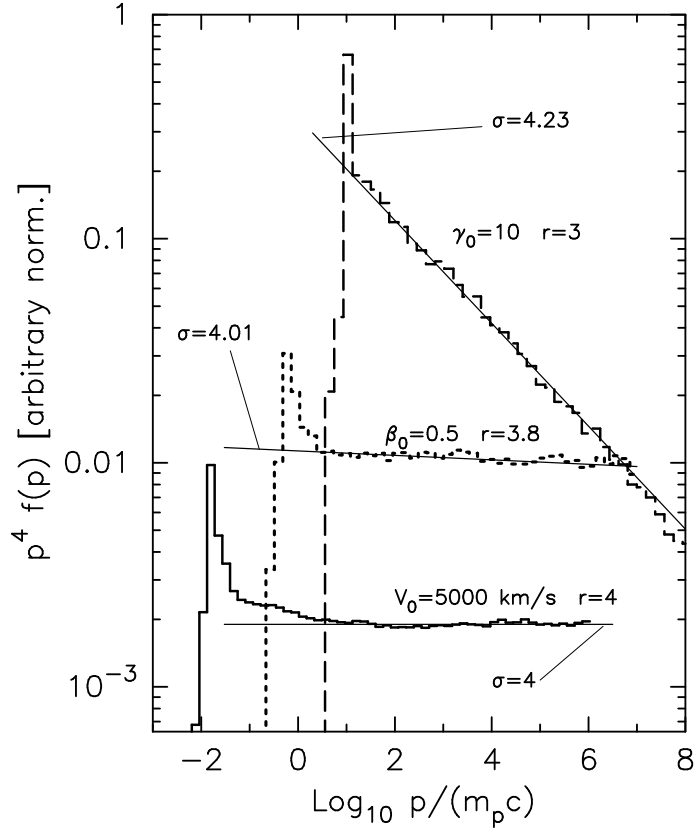


Fig. 3.— Particle spectra, $p^4 f(p)$, versus momentum for various unmodified shocks with speeds as indicated. The test-particle compression ratios, r , and spectral indices, σ , are noted. The far upstream plasmas in the 5000 km s⁻¹, and $\beta_0 = 0.5$ shocks are thermal at 10⁶ K. The $\gamma_0 = 10$ shock has a far upstream plasma which is a δ -function at 1 MeV. All spectra are calculated at the shock, in the shock frame, and the relative normalization is arbitrary.

accelerated particles. This technique is described in detail in Ellison & Reynolds (1991). We find $r = 3.8 \pm 0.1$ and the spectral index is $\sigma \simeq 4.01$, slightly flatter than $3r/(r-1) \simeq 4.07$, the nonrelativistic result.

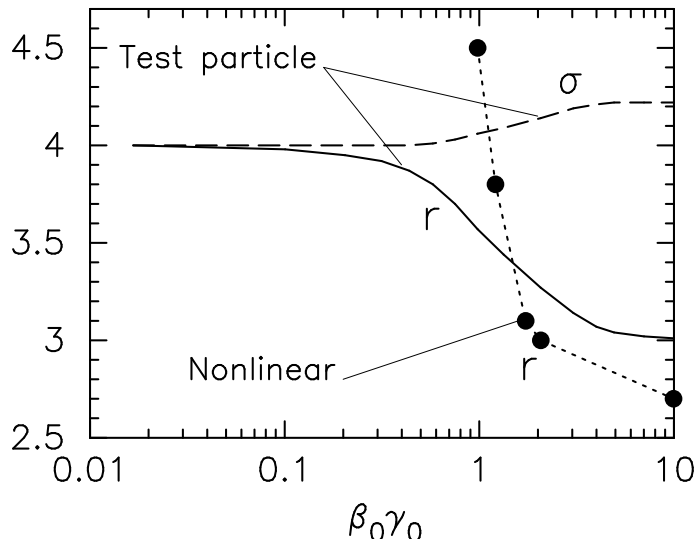


Fig. 4.— The solid line is the compression ratio, r , and the dashed line is the spectral index, σ , for unmodified (i.e., test-particle) shocks. The solid dots show r for shocks undergoing efficient particle acceleration. In all cases, r is determined for each $\beta_0\gamma_0$ by balancing the momentum and energy fluxes across the shock.

Figure 4 shows the compression ratio as a function of $\beta_0\gamma_0$ (solid curve), still ignoring the effects of accelerated particles. As expected, r decreases smoothly from 4 for fully nonrelativistic shocks to ~ 3 for fully relativistic shocks. The power law index, σ , is also shown (dashed curve, top panel) and this varies slowly from $\sigma = 4$ to $\sigma \simeq 4.23$ between the two extremes. For comparison, we show r (solid dots) for shocks undergoing efficient particle acceleration. For these points, all shock parameters (particularly $p_{\max} = 3.2 \times 10^4 m_p c$)⁵ are kept constant except $\beta_0\gamma_0$, which is varied as shown. The shocks with $\gamma_0 = 1.4, 2.3$, and 10 are discussed in detail below, but here we only emphasize that r in nonlinear shocks will be larger than the test-particle value at low γ_0 and fall below the test-particle above some critical γ_0 .

In Figure 5 we show the average ratios of momenta (measured in the local plasma frame) for particles executing upstream to downstream to upstream cycles across the shock, $\langle p_f/p_i \rangle_{u-d-u}$, and downstream to upstream to downstream cycles, $\langle p_f/p_i \rangle_{d-u-d}$. These results are for $\gamma_0 = 10$ ($r = 3$) and show a slight momentum dependence at low momenta but converge to $\langle p_f/p_i \rangle =$

⁵The maximum cutoff momentum has a small influence on the shock characteristics at low $\beta_0\gamma_0$ because r is large enough that particles escaping at p_{\max} are dynamically important. When $\beta_0\gamma_0$ becomes large enough so that r drops below ~ 4 , p_{\max} is no longer an important parameter for the shock structure.

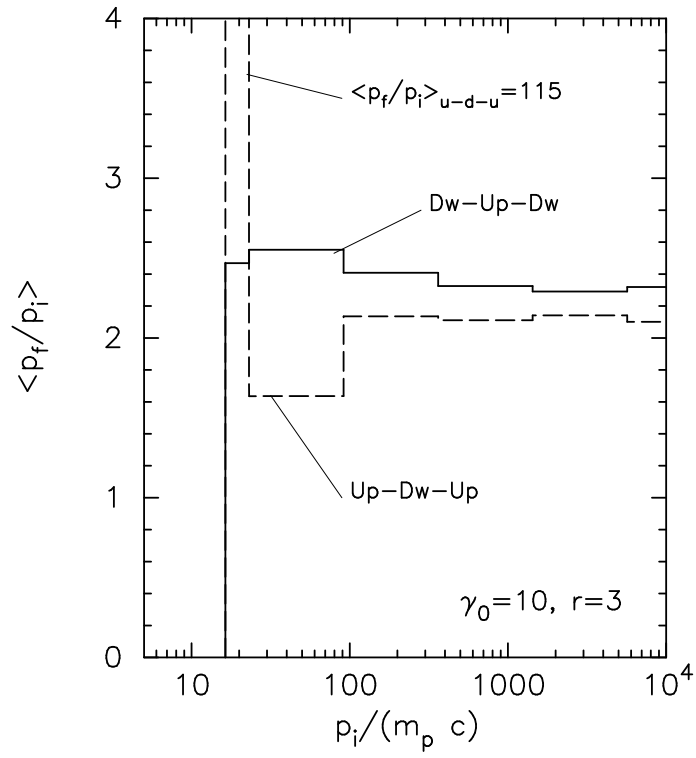


Fig. 5.— Average ratios of final (f) to initial (i) momentum for downstream to upstream to downstream and upstream to downstream to upstream shock crossing cycles. The histograms are for a test-particle shock with $\gamma_0 = 10$ and $r = 3$. Note the large momentum gain ($\langle p_f/p_i \rangle_{u-d-u} = 115$) in the first shock crossing cycle.

2.2 ± 0.1 at high momenta. This value is close to $\langle E_f/E_i \rangle = 1.97 \pm 0.01$ reported by Achterberg et al. (2001) for $\gamma_0 = 10$. As mentioned above, in the first upstream to downstream to upstream cycle, particles achieve a large boost in momentum as indicated in the figure.

The difference between our value of $\langle p_f/p_i \rangle$ at large p_i and that of Achterberg et al. (2001) is greater than the uncertainties and probably stems from the different assumptions made in the simulations. As discussed above, $\langle p_f/p_i \rangle$ depends critically on the average angle a particle makes when crossing the shock. While the large majority of particles in our simulations gain energy by crossing from downstream to upstream and then immediately (within a few δt 's) re-crossing back into the downstream region at oblique angles, a few manage to diffuse farther upstream (see Figure 7 below). When these particles re-cross the shock into the downstream region, they can do so at flatter angles and receive larger energy gains. We speculate that differences in how these few particles are treated in the simulations might produce the differences in $\langle p_f/p_i \rangle$.

As an illustration of how particles interact with nonrelativistic and relativistic unmodified, we shown trajectories for two individual particles in Figures 6 and 7. The lower panel in each figure shows a trace of the particle trajectory and the upper panels show the particle momentum, always measured in the local plasma frame. For the nonrelativistic shock (Figure 6), the speed of the particle is far greater than the shock speed and it diffuses easily on both sides of the shock. When it crosses $x = 0$, it does so nearly isotropically (except flux weighting makes crossings with flat trajectories slightly more likely) and essentially always gains momentum. The momentum gain in a single shock crossing is small, but a particle can stay in the system for many crossings.

When the shock speed, u_0 , is close to c , the particle will be convected downstream much more rapidly than in nonrelativistic shocks and few particles will be able to cross the shock many times. However, downstream particles that do manage to cross the shock into the upstream region do so with much flatter trajectories, as discussed above, and can receive large momentum boosts in a single shock crossing due to the shock's Lorentz factor (note the logarithmic scale in the top panel of Figure 7). In a typical shock crossing cycle, downstream particles gain momentum when they cross into the upstream region (see positions labeled *a* and *b* in Figure 7), lose momentum when they cross back downstream because they cross with oblique pitch angles, but end up with a net momentum boost. However, as shown by the position labeled *c*, it is possible for a particle to diffuse farther upstream before being convected back to the shock. In this case, it can cross the shock with a flat trajectory and gain momentum upon entering the downstream region. If the acceleration is efficient, the few particles that diffuse far upstream carry enough pressure to produce the shock smoothing we discuss next.

4. Non-Linear Results

As noted by Achterberg et al. (2001), the large energy boost particles receive in their initial crossing of the shock provides a natural injection process for further acceleration and suggests that

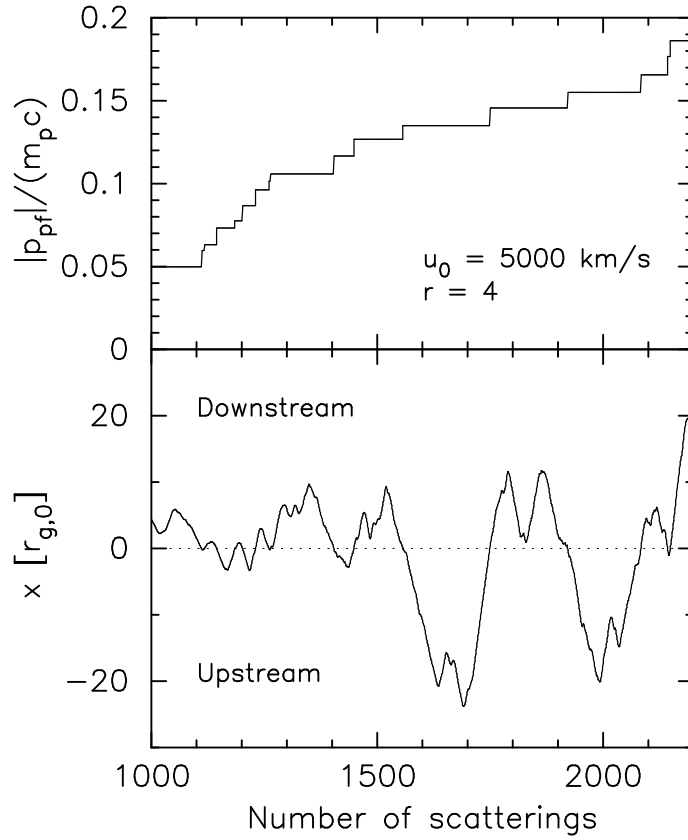


Fig. 6.— Particle trajectory (lower panel) and momentum (upper panel) in an unmodified shock of speed $u_0 = 5000 \text{ km s}^{-1}$. The momentum is calculated in the local plasma frame, either upstream or downstream from the shock.

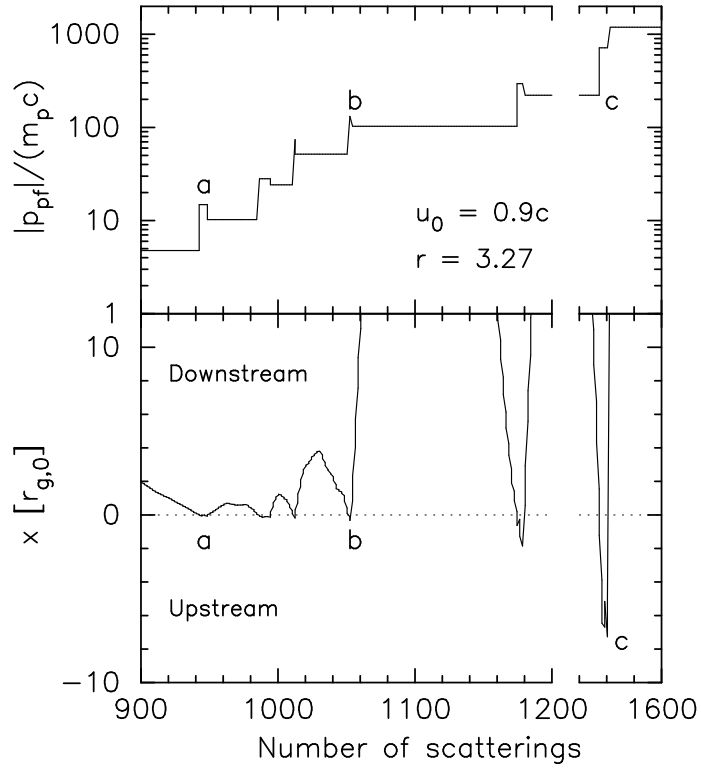


Fig. 7.— Trajectory and momentum for a particle in an unmodified shock with speed $u_0 = 0.9c$. Note that the horizontal axis is split at 1200 scatterings.

relativistic shocks may be efficient accelerators. However, just as with nonrelativistic shocks, efficient acceleration limits the use of test-particle approximations and requires that the nonlinear backreaction of the accelerated particles be treated self-consistently (e.g., Jones & Ellison 1991). These nonlinear effects will result in a smoothing of the shock and a change in the overall shock compression ratio, just as they do in nonrelativistic shocks. The differences between test-particle and nonlinear results, for all of the parameter ranges we have investigated, are large enough to produce spectra noticeably different from the often quoted $N(E) \propto E^{-2.3}$ and to influence applications to GRB models where high shock efficiencies are assumed. We illustrate this with two examples, one mildly relativistic ($\gamma_0 = 1.4$) and one more fully relativistic ($\gamma_0 = 10$). The far upstream conditions have relatively little influence on our results as long as $\gamma_p \ll \gamma_0$, where γ_p is the plasma frame Lorentz factor of the far upstream, injected particles. For concreteness, in both examples we take the far upstream plasma to be a thermal distribution of electrons and protons at a temperature of 10^6 K, but we only consider proton acceleration; the electrons only being included for charge neutrality.

4.1. Mildly relativistic shock: $\gamma_0 = 1.4$

Figure 8 shows unmodified and nonlinear shock structures for $\gamma_0 = 1.4$. The top panel shows $\gamma_u(x) u(x)$, where $\gamma_u(x) = \{1 - [u(x)/c]^2\}^{-1/2}$, the middle panel is momentum flux, and the bottom panel is the energy flux, all scaled to far upstream values. All curves are plotted versus x , where $x = 0$ is the position of the sharp subshock. A logarithmic scale is used for $x < -10r_{g,0}$ and a linear scale is used for $x > -10r_{g,0}$, where $r_{g,0} \equiv m_p u_0 / (eB)$. In each panel, the solid curve is from an unmodified shock with $r \simeq 3.6$ (see Figure 4), while the dashed curve is the momentum and energy flux conserving result.

For our pitch angle diffusion model, where particles interact elastically and isotropically in the local frame according to equation (2) and the discussion following it, particles are accelerated efficiently enough at the unmodified shock that the momentum and energy fluxes are not conserved and rise well above the allowed far upstream values. In order to conserve these fluxes, the shock structure must be smoothed and the overall compression ratio increased above the test-particle value. Our computational scheme calculates this compression ratio and flux conserving profile and the result is the dashed curve in the top panel with the corresponding momentum and energy fluxes in the middle and bottom panels.

The source of the non-conservation of momentum and energy is the efficient acceleration of particles by the sharp flow speed discontinuity. While the actual injection and acceleration efficiency depends on our particular pitch angle diffusion model, once our scattering assumptions are made, the kinematics determine the injection and acceleration of the particles without additional

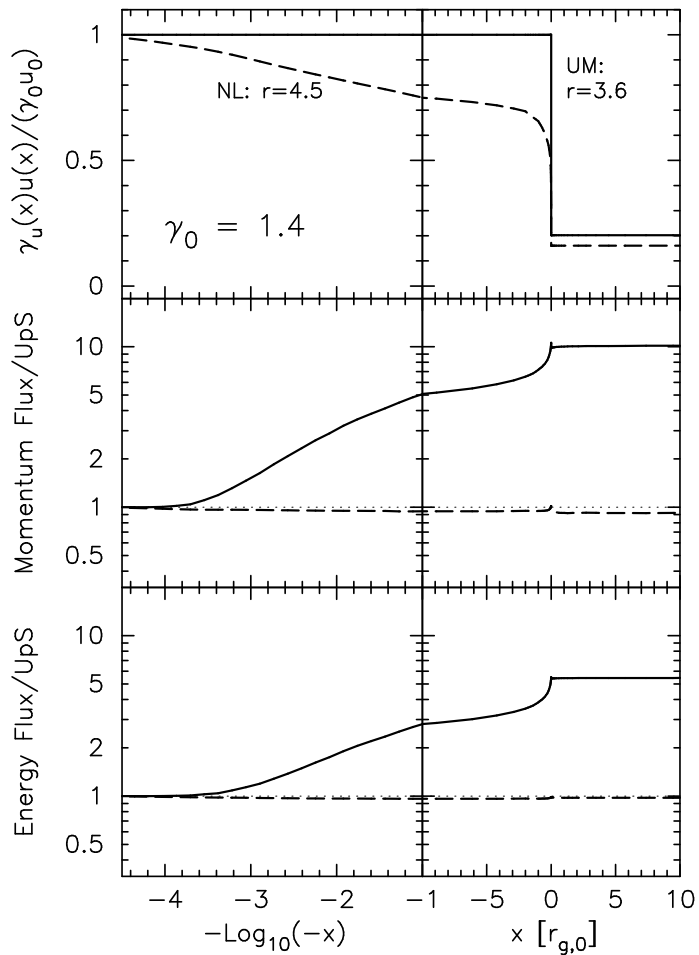


Fig. 8.— Unmodified (UM) and nonlinear (NL) shock profiles, i.e., $\gamma_u(x)u(x)$, and momentum and energy fluxes versus position, x . All quantities are scaled to far upstream values and in all panels the solid curves are results from unmodified shocks and the dashed curves are nonlinear results. The NL momentum and energy fluxes are 3 to 4% below the far upstream values because particles escape at a maximum momentum, $p_{\text{max}} = 3.2 \times 10^4 m_p c$. We have used $N/N_{\text{min}} \sim 10$ in both cases.

parameters.⁶ Of course it would have been possible to make assumptions which resulted in an acceleration efficiency low enough that momentum and energy are approximately conserved without significantly smoothing the shock structure or changing the compression ratio from the test-particle value. For example, we could have only allowed shocked particles above some Lorentz factor γ_{inj} to recross into the upstream region or arbitrarily restricted the number of particles that recrossed into the upstream to a small fraction, f_{inj} , of all downstream particles. By making f_{inj} low enough or γ_{inj} high enough we could make the efficiency as low as we wanted. However, there are at least three reasons for not making such an assumption. The first is that restricting the acceleration efficiency requires additional parameters (i.e., γ_{inj} and/or f_{inj}) to those needed to describe pitch angle diffusion.⁷ The second is that models with *inefficient* acceleration will not help explain GRBs (or other objects) that require high efficiencies. If relativistic shocks are inefficient accelerators they are not very interesting. If they are efficient, they will have a qualitative resemblance to the results we show even if, as is likely, the actual plasma processes are far more complex than the simple model we use. The third, perhaps less compelling, reason is that identical scattering assumptions as used here have been used for some time in nonrelativistic shocks and shown to match both spacecraft observations (e.g., Ellison, Möbius, & Paschmann 1990) and hybrid plasma simulations (e.g., Ellison et al. 1993) of collisionless shocks.

The increase in compression ratio from $r \simeq 3.6$ to $\simeq 4.5$ shown in Figure 8 comes about, in part, because the particles escaping at p_{max} carry away momentum and energy fluxes which make the shocked plasma more compressible. This effect is countered to some degree by the fact that the self-consistent shock produces a downstream distribution with a smaller fraction of relativistic particles than the test-particle shock so that the downstream ratio of specific heats $\Gamma > 4/3$. This tends to produce a smaller compression ratio. The escaping fluxes show up as a lowering of the dashed curves below the far upstream values, as shown in the bottom two panels of Figure 8, and amount to about 3% of the far upstream values for both momentum and energy. Including the escaping fluxes, the momentum and energy fluxes are conserved to within a few percent of the far upstream values. While the changes seen here are similar to those seen and discussed for many years in efficient, nonrelativistic shock acceleration (see Berezhko & Ellison 1999, and references therein), it must be noted that there are no known analytic expressions relating escaping fluxes and Γ to r in this trans-relativistic regime. One obvious difference is that for nonrelativistic shocks, the escaping momentum flux is generally much less than the escaping energy flux (when both are measured as fractions of incoming flux) since $\rho_e v_e^3 / (\rho_0 u_0^3) \gg \rho_e v_e^2 / (\rho_0 u_0^2)$ when $v_e \gg u_0$ (see Ellison 1985). Here, v_e is the velocity of the escaping particle. In relativistic shocks, $v_e \sim u_0 \sim c$ so the escaping fluxes are about equal as shown in Figure 8.

⁶Other input parameters, such as the Mach number and p_{max} or the position of the FEB, influence the acceleration efficiency, but these are “environmental” parameters rather than parameters needed to describe the plasma interactions.

⁷Alternatively, a far more complex model of the plasma interactions can be postulated than done here, inevitably requiring additional parameters (e.g., Malkov 1998).

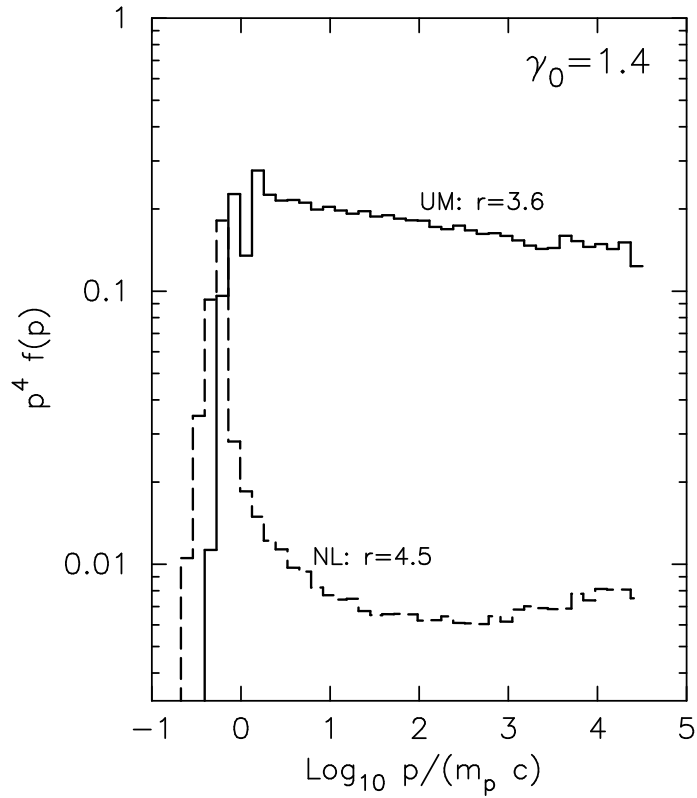


Fig. 9.— Particle distributions, $p^4 f(p)$, for the shocks shown in Figure 8. The nonlinear spectrum (dashed curve) shows the distinctive concave shape seen in efficient nonrelativistic shock acceleration, and has a greater fraction of low momentum particles than the spectrum from the unmodified shock. As in Figure 3, the spectra are calculated at the shock in the shock frame and truncated with a p_{max} . Unlike Figure 3, the normalization here shows the actual acceleration efficiency.

In Figure 9 we plot $p^4 f(p)$ for our $\gamma_0 = 1.4$ shock. The solid curve is from an unmodified (UM) shock and the dashed curve is the nonlinear (NL) result. The shock smoothing and increase in r produce substantial differences in the spectra even though both shocks have exactly the same input conditions. (i) The overall normalization of the NL spectrum is less, reflecting the conservation of energy flux. (ii) The NL result has the distinctive concave curvature seen in nonrelativistic shocks stemming from the fact that higher momentum particles have a longer upstream diffusion length and get accelerated more efficiently than lower momentum particles in the smooth shock. (iii) The slope at the highest momentum in the NL spectrum reflects the overall compression ratio and is flatter than the TP spectrum because r is greater. (iv) The “thermal” peak is shifted to lower momentum in the NL result and contains a larger fraction of mildly relativistic particles than in the UM result, i.e., $\Gamma \simeq 1.41$ for the NL shock compared to $\Gamma \simeq 1.36$ for the UM shock.

4.2. Fully relativistic, nonlinear shock: $\gamma_0 = 10$

Fully relativistic shocks have a decidedly different behavior from nonrelativistic or mildly relativistic ones. Figure 10 shows results for an unmodified shock (solid curves) along with a flux conserving one where the shock has been smoothed and the compression ratio has been *reduced* to $r \simeq 2.7 \pm 0.05$. For variation, we have truncated the acceleration with an upstream FEB at $x = -100r_{g,0}$ rather than a p_{\max} , as was the case for the examples shown in Figures 8 and 9. This change has no important effect on the NL aspects of the result, but does produce an approximately exponential drop off in the spectrum at high momenta, as discussed below.

The change in r shows up clearly in the top panel of Figure 11 where $u(x)$ and $\gamma_u(x)$ are plotted separately. The compression ratio drops in the NL shock because the smooth shock produces a larger fraction of mildly relativistic particles than the test-particle shock, i.e., the ratio of specific heats, Γ , is greater in the shocked plasma in the NL shock. The steep spectrum results in too few escaping particles to overcome the effect from the change in Γ . The influence of Γ on r can be seen by considering the relativistic jump conditions for momentum and energy, i.e.,

$$\gamma_{u0}^2 w_0 \frac{u_0^2}{c^2} + P_0 = \gamma_{u2}^2 w_2 \frac{u_2^2}{c^2} + P_2 ; \quad (9)$$

$$\gamma_{u0}^2 w_0 u_0 = \gamma_{u2}^2 w_2 u_2 , \quad (10)$$

where $w = e + P$ is the enthalpy density, e is the total energy density, and P is the pressure. The energy density and pressure are related through a combination of the adiabatic equation of state and the conservation of energy, i.e.,

$$P = (\Gamma - 1)(e - \rho c^2) , \quad (11)$$

where ρc^2 is the rest mass energy density and Γ is, in special cases, the ratio of specific heats (e.g., Ellison & Reynolds 1991).

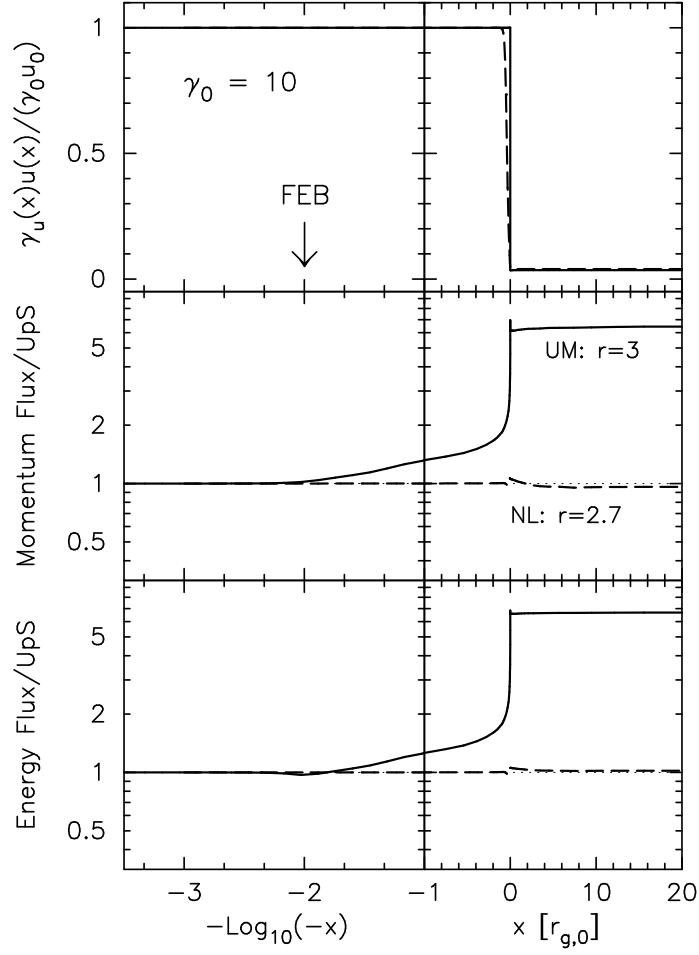


Fig. 10.— Unmodified (UM: solid curves) and nonlinear (NL: dashed curves) shock profiles as in Figure 8 for $\gamma_0 = 10$. The acceleration is truncated by a free escape boundary at $x = -100 r_{g,0}$. We have used $N/N_{\min} \sim 10$ in both cases.

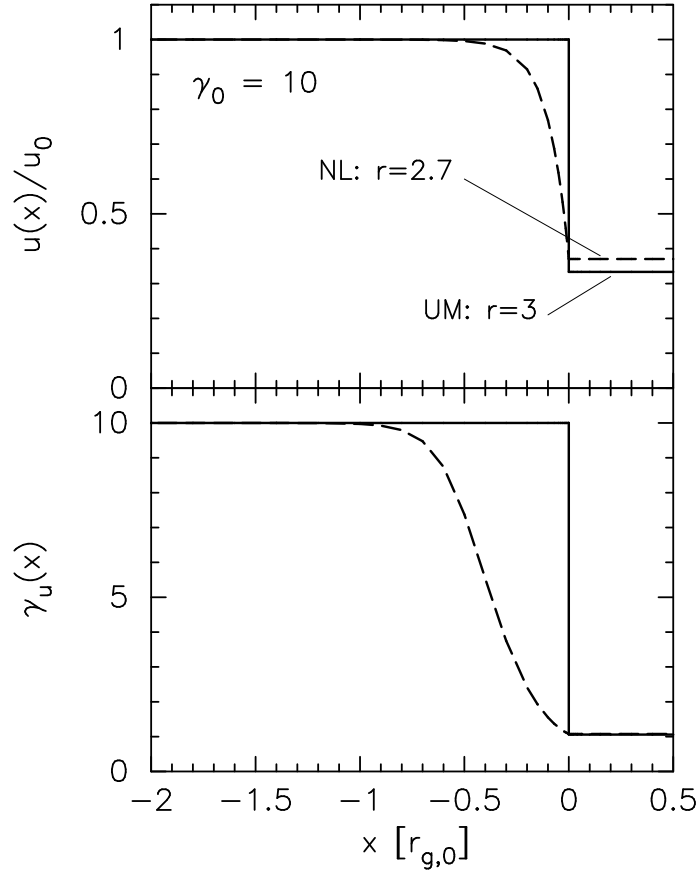


Fig. 11.— The top panel is the flow speed at x normalized to the far upstream shock speed, u_0 versus x , for the $\gamma_0 = 10$ shocks shown in Figure 10. The bottom panel is the flow Lorentz factor, $\gamma_u(x)$, versus x . In both panels, the solid curves are the unmodified shock results with $r = 3$ and the dashed curves are the nonlinear results with $r \simeq 2.7 \pm 0.05$.

In the ultrarelativistic regime $e \gg \rho c^2$, so

$$P \simeq (\Gamma - 1)e \quad (12)$$

and

$$w \simeq e + (\Gamma - 1)e = \Gamma e . \quad (13)$$

Dividing equation (9) by equation (10), we have,

$$\frac{u_o}{c^2} + \frac{(\Gamma_0 - 1)}{\gamma_{u0}^2 \Gamma_0 u_0} = \frac{u_2}{c^2} + \frac{(\Gamma_2 - 1)}{\gamma_{u2}^2 \Gamma_2 u_2} , \quad (14)$$

or, in terms of beta's

$$\beta_0 + \left(\frac{\Gamma_0 - 1}{\Gamma_0} \right) \frac{1 - \beta_0^2}{\beta_0} = \beta_2 + \left(\frac{\Gamma_2 - 1}{\Gamma_2} \right) \frac{1 - \beta_2^2}{\beta_2} . \quad (15)$$

Equation (15) shows that when the shock speed is close to c ($\beta_0 \simeq 1$), the compression ratio, $r = \beta_0/\beta_2$, is approximately independent of the upstream Γ_0 . In this limit,

$$\beta_2^2 - \Gamma_2 \beta_2 + (\Gamma_2 - 1) = 0 \quad (16)$$

and

$$\beta_2 = 1/r = (\Gamma_2 - 1) . \quad (17)$$

If the shocked $\Gamma_2 = 4/3$, the standard ultrarelativistic result of $r = 3$ is obtained. If $\Gamma_2 > 4/3$, r will decrease below 3 as we see happening in Figures 4 and 10.

Despite the fact that $\gamma_u(x)u(x)$ seems barely modified in Figure 10, the changes in shock structure and decrease in r show up in the resultant particle distribution function, as indicated in Figure 12. In this figure, the solid curve is the test-particle result and the dashed curve is the nonlinear result, both having exactly the same input conditions. The test-particle curve in Figure 12 is similar to that shown with a dashed curve in Figure 3 only now a FEB limits the maximum particle energy and the far upstream plasma is a thermal gas at a temperature of 10^6 K rather than a delta function distribution of particles with speeds, $v_{\text{inj}} = (2E_{\text{inj}}/m_p)^{1/2}$, with $E_{\text{inj}} = 1$ MeV, as assumed for the example in Figure 3. The FEB acts differently from a cutoff at p_{max} only in that escaping particles have a range in momentum which produces an approximately exponential turnover in $f(p)$.

The decrease in r has caused the power law portion of the distribution to steepen and it now has $\sigma \simeq 4.45$. The overall intensity is also lower reflecting the fact that the NL spectrum conserves momentum and energy while the UM one doesn't. The peaks in the two distributions at low momenta are also very different, with the NL spectrum having a larger fraction of slower particles than the UM one. These peaks result from the first shock crossing where all particles receive a large energy gain. In the UM case, a far greater fraction of the accelerated downstream particles are able to receive further energization by recrossing back into the upstream region than in the NL

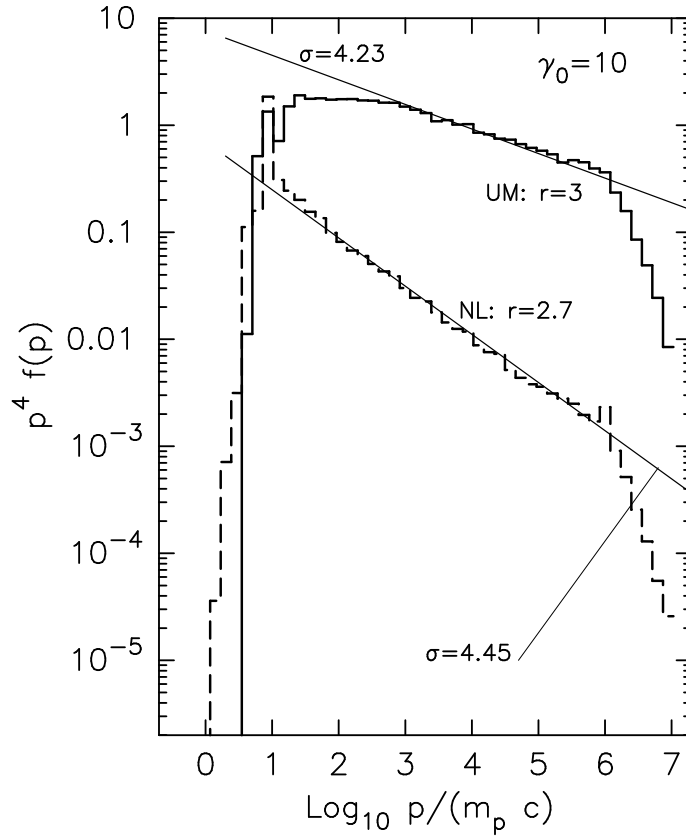


Fig. 12.— Particle distributions, $p^4 f(p)$, for the shocks shown in Figures 10 and 11 with $\gamma_0 = 10$. The spectra for the nonlinear (NL) and unmodified (UM) shocks are labeled and both are calculated at $x = 0$ in the shock frame. These spectra are truncated with a FEB at $x = -100 r_{g,0}$.

shock. The different speed distributions result in different Γ 's and we find, by directly calculating Γ from the distributions, that $\Gamma_{\text{UM}} \simeq 1.34$ while $\Gamma_{\text{NL}} \simeq 1.36$. With this Γ_{NL} , equation (17) predicts $r \simeq 2.8$, within 3% of $r = 2.7 \pm 0.05$ found from balancing the momentum and energy fluxes.

It's clear from our $\gamma_0 = 1.4$ and 10 results that a transition between $r > r_{\text{TP}} = 3$ and $r < r_{\text{TP}}$ must occur. This comes about because the particle spectrum steepens as γ_0 increases from $\gtrsim 1$ and escape becomes less important. At some γ_0 , the tendency for r to increase because of escape is balanced by the decrease caused by the increase in Γ . We have determined the transition Lorentz factor giving $r \simeq 3$ to be $\gamma_{\text{tr}} \simeq 2.3$, a value quite insensitive to the far upstream conditions (as long as $\gamma_p \ll \gamma_{\text{tr}}$) or to the maximum particle momentum obtained (i.e., to p_{max} or the position of the FEB). The fact that γ_{tr} is not far above $\gamma_0 = 1.4$, which gave a self-consistent solution with $r \simeq 4.5$, is an indication of the strength of the nonlinear effects from particle escape. Once r increases because of escaping flux, the spectrum becomes flatter, creating even more escaping flux and a larger r , etc.

4.3. Acceleration efficiency

The absolute acceleration efficiency can be determined in our self-consistent, nonlinear examples directly from the particle distributions. In Figure 13 we plot, $\epsilon(> p)$, the fraction of kinetic energy density above a momentum p versus p for our $\gamma_0 = 1.4$ and $\gamma_0 = 10$ examples. The fraction of kinetic energy in the quasi-thermal part of the distribution can be determined from the relatively sharp fall off of the distributions at low momenta. This occurs near $m_p c$ for $\gamma_0 = 1.4$ and near $10 m_p c$ for $\gamma_0 = 10$. If we somewhat arbitrarily define the acceleration efficiency for these two examples to be $\epsilon_{1.4}(> m_p c)$ and $\epsilon_{10}(> 20 m_p c)$, respectively, we have $\epsilon_{1.4}(> m_p c) \simeq 0.7$ and $\epsilon_{10}(> 20 m_p c) \simeq 0.3$. Of course, the behavior of $\epsilon(> p)$ depends on the particle spectrum from which it is derived and thus $\epsilon(> p)$ is much flatter for the $\gamma_0 = 1.4$ shock, with $r \simeq 4.5$, than for the $\gamma_0 = 10$ shock, where $r \simeq 2.7$. Furthermore, $\epsilon(> p)$ depends strongly on the maximum momentum in the $\gamma_0 = 1.4$ shock (set by either p_{max} or a FEB) since in this case particle escape plays an important role in determining r . The maximum momentum has little influence for $\gamma_0 = 10$ because of the steep spectrum and less than 5% of the total kinetic energy density lies above $10^3 m_p c$ in this case. The acceleration efficiency for the transition Lorentz factor, γ_{tr} , is shown in Figure 13 as a dotted line and in this case, approximately 40% of the total kinetic energy density lies above the thermal peak.

5. Summary and Conclusions

Particles gain energy in collisionless shocks by scattering nearly elastically off magnetic turbulence, back and forth between the converging plasmas upstream and downstream from the shock. While this basic shock acceleration physics is independent of the speed of the shock, the mathematical modeling of the process depends critically on whether or not the acceleration is efficient

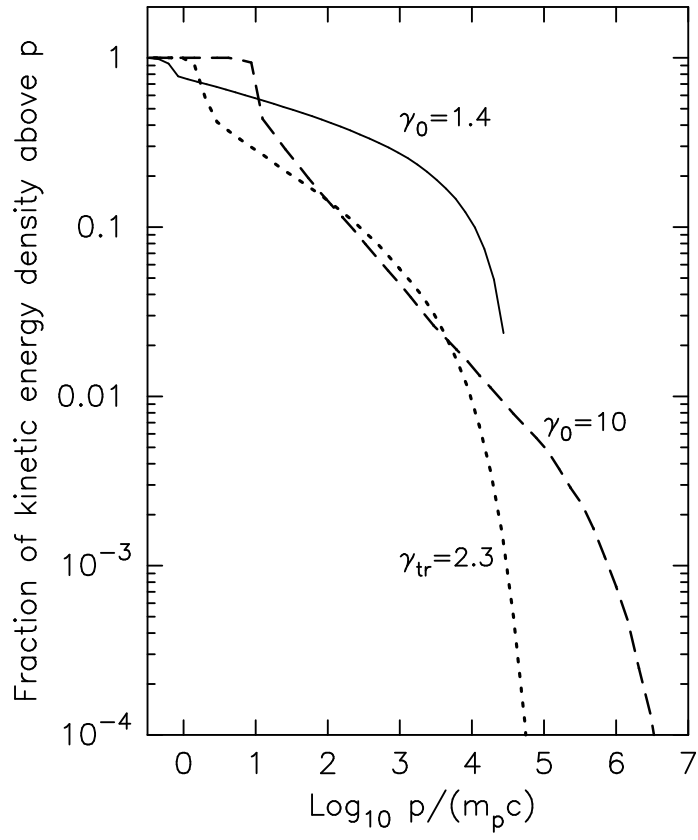


Fig. 13.— Acceleration efficiency, $\epsilon(> p)$, defined as the fraction of total kinetic energy density above p versus p . The sharp drop off at low momenta indicates the extent of the ‘thermal’ peak.

and whether or not particle speeds, v , are large compared to the shock speed, u_0 . Monte Carlo techniques, which do not require $v \gg u_0$, are well suited for the study of relativistic shocks, and for any shock where nonlinear effects are important and the energetic particles originate as thermal particles in the unshocked plasma. Except for computational limits, these techniques allow calculations of efficient particle acceleration in shocks of any Lorentz factor.

As a check of our code, we have demonstrated that we obtain the well known, test-particle power laws in fully nonrelativistic and ultrarelativistic shocks (Figures 1 and 3). In trans-relativistic shocks, however, no such canonical results exist because the shock compression ratio, r , depends on the upstream conditions in a nonlinear fashion, even for test-particle shocks where all effects of accelerated particles are ignored (e.g., Ellison & Reynolds 1991). We show how r , and the resulting power law spectral index, σ , vary through the trans-relativistic regime in Figure 4, where r has been determined by balancing the momentum and energy fluxes across the shock in an iterative process. To our knowledge, this is the first presentation of power law indexes obtained for trans-relativistic shocks with self-consistent compression ratios.

Despite the fact that relativistic shock theory has concentrated almost exclusively on test-particle acceleration, it is likely that relativistic shocks are not test-particle but inject and accelerate particles efficiently. The reason is that regardless of the ambient far upstream conditions, particles that are overtaken by an ultrarelativistic shock will receive a large boost in energy $\sim \gamma_0$ in their first shock crossing. Thus, virtually all of the particles in the downstream region of an unmodified shock are strongly relativistic with $v \sim c$. The ability to overtake the shock from downstream and be further accelerated depends only on the particle speed (equation 7) and the presence of magnetic waves or turbulence with sufficient power in wavelengths on the order of the particle gyroradii to isotropize the downstream distributions. It is generally assumed that the necessary magnetic turbulence is self-generated and if enough turbulence is generated to scatter high momentum particles (with very low densities) that constitute a test-particle power law, there should be enough generated to isotropize lower momentum particles (which carry the bulk of the density). If acceleration can occur at all, it is likely to occur efficiently making it necessary to calculate the shock structure and particle acceleration self-consistently. Furthermore, if relativistic shock theory is to be applied to gamma ray bursts, where high conversion efficiencies are generally assumed, nonlinear effects must be calculated.

When energetic particles are generated in sufficient numbers, the conservation of momentum and energy requires that their backpressure modify the shock structure. Two basic effects occur: a precursor is formed when the upstream plasma is slowed by the backpressure of the accelerated particles and the overall compression ratio changes from the test-particle value as a result of high energy particles escaping and/or a change in the shocked plasma's ratio of specific heats, Γ . As indicated by our $\gamma_0 = 1.4$ example (Section 4.1), mildly relativistic shocks act as nonrelativistic ones showing a dramatic weakening of the subshock combined with a large increase in r (Figure 8). These changes result in a particle distribution which is both steeper than the test-particle power law at low momenta and flatter at high momenta (Figure 9).

In fully relativistic shocks, the initial test-particle spectrum is steep enough that particle escape is unimportant, and $\Gamma \sim 4/3$, making it impossible for r to increase above the test-particle value of 3. However, the shock smoothing necessary to reduce the acceleration efficiency and conserve momentum and energy, also produces fewer fully relativistic particles causing Γ to increase. A consistent solution is found with $r < 3$, as shown in Figure 10. For our $\gamma_0 = 10$ example, the lower r results in a spectrum with a power law index of $\sigma \simeq 4.45$, somewhat steeper than the test-particle result with $\sigma \simeq 4.23$ (Figure 12). A transition between $r > r_{\text{TP}} = 3$ and $r < r_{\text{TP}}$ occurs at $\gamma_{\text{tr}} \simeq 2.3$.

Our most important result is that efficient shocks, whether mildly or fully relativistic, do not necessarily produce particle spectra close to the so-called ‘universal’ power law having $\sigma \sim 4.3$, except for a small range of shock Lorentz factors around γ_{tr} . Due to computational limits, we have not yet fully investigated extremely high γ_0 shocks undergoing efficient acceleration. However, from our initial results we estimate that once $\gamma_0 \gtrsim 50$, a shock can conserve momentum and energy by smoothing with no change in r from the test-particle value of 3.

The authors thank M. G. Baring, L. O’C. Drury, F. C. Jones, and E. Parizot for helpful discussions. D.C.E. is grateful to the Department of Physics and Astronomy at Rice University and to the Dublin Institute for Advanced Studies for hosting visits where part of this work was done.

REFERENCES

- Achterberg, A., Gallant, Y. A., Kirk, J. G., & Guthmann, A. W. 2001, *M.N.R.A.S.*, 328, 393
- Axford, W. I., Leer, E., & Skadron, G. 1977, in *Proc. 15th ICRC(Plovdiv)*, 11, 132
- Bednarz, J., & Ostrowski, M. 1996, *M.N.R.A.S.*, 283, 447
- Bednarz, J. & Ostrowski, M. 1998, *Phys. Rev. Letts*, **80**, 3911
- Berezhko, E. G., & Ellison, D. C. 1999, *ApJ*, 526, 385
- Berezhko, E. G., & Völk, H. J. 1997, *Astroparticle Phys.*, 7, 183
- Blandford, R. D., & Eichler, D, 1987, *Physics Reports*, 154, 1
- Blandford, R. D. & McKee, C. F. 1976, *Phys. Fluids*, 19 #8, 1130
- Blandford, R.D., & Ostriker, J.P., 1978, *ApJ*, 221, L29
- Drury, L. O’C. 1983, *Rep. Prog. Phys.*, 46, 973
- Ellison, D. C. 1985, *J.G.R.*, 90, 29

- Ellison, D. C. 1991a, Proc. ICRR International Symposium on “Astrophysical Aspects of the Most Energetic Cosmic Rays,” p. 281, Eds., M. Nagano and F. Takahara, World Scientific, Bangalore.
- Ellison, D. C. 1991b, in “Relativistic Hadrons in Cosmic Compact Objects,” p. 101, Eds., A. A. Zdziarski and M. Sikora, Springer-Verlag, Berlin.
- Ellison, D. C., Baring, M. G., & Jones, F. C. 1996, *ApJ*, 473, 1029
- Ellison, D. C., & Eichler, D. 1984, *ApJ*, 286, 691
- Ellison, D. C., Giacalone, J., Burgess, D., and Schwartz, S. J., 1993, *J.G.R.*, 98, 21,085
- Ellison, D. C., Jones, F. C., & Baring, M. G. 1999, *ApJ*, 512, 403
- Ellison, D.C., Jones, F.C., and Reynolds, S.P., 1990, *ApJ*, 360, 702
- Ellison, D.C., Möbius, E., & Paschmann, G., 1990, *ApJ*, 352, 376
- Ellison, D. C., & Reynolds, S. P. 1991, *ApJ*, 378, 214
- Gallant, Y. A. & Achterberg, A. 1999, *M.N.R.A.S.*, 305, L6
- Heavens, A. F. & Drury, L. O’C. 1988, *M.N.R.A.S.*, 235, 997
- Jones, F.C., & Ellison, D.C. 1991, *Space Sci. Rev.*, 58, 259
- Kirk, J. G. 1988, Thesis, Dr. rer. nat. habil., Ludwig-Maximilians-Universität, München, Germany.
- Kirk, J. G., Guthmann, A. W., Gallant, Y. A., Achterberg, A. 2000, *ApJ*, 542, 235
- Kirk, J. G. & Schneider, P. 1987a, *ApJ*, 315, 425
- Kirk, J. G., & Schneider, P. 1987b, *ApJ*, 322, 256
- Malkov, M. 1998, *Phys. Rev. E*, **58**, 4911
- Ostrowski, M., 1991, *M.N.R.A.S.*, 249, 551
- Peacock, J. A. 1981, *M.N.R.A.S.*, 196, 135
- Pelletier, G. 1999, *A&A*, 350, 705
- Pelletier, G., & Marcowith, A. 1998, *ApJ*, 502, 598
- Schneider, P. & Kirk, J. G. 1987, *ApJ*, 323, L87
- Vietri, M., 1995, *ApJ*, 453, 883